An experimental investigation of a low Reynolds number turbulent boundary layer subject to an adverse pressure gradient

By J. H. Watmuff

The evolution of a low Re_θ turbulent boundary layer in an adverse pressure gradient (APG) is being studied for comparison with direct numerical simulations by Spalart. A short region of favorable pressure gradient (FPG) is applied first to establish a self-preserving layer with $Re_\theta \approx 600$, which is a suitable initial condition for the simulations. The APG is then applied rapidly such that $\beta \approx 2$ at $Re_\theta \approx 1500$. The streamwise extent of the measurements exceeds the current capabilities of direct simulations so that the results should also serve as a useful data base for Reynolds-averaged boundary layer prediction methods and in the future for direct simulation schemes as computer technology evolves.

1. Relationship between the experiment and CFD simulations

An important feature of the numerical method of Spalart (1988) is that there is no turbulence modelling. A high non-dimensional grid density is needed which restricts the simulations to low Reynolds numbers, i.e. $R_\theta < 1500$ at present. The key assumptions in Spalart's 1988 method are that the streamwise evolution of the flow is slow and that the straining of the turbulence by the mean-flow can be neglected. These assumptions will inevitably cause the method to breakdown in a large APG. Spalart has developed a new technique that should overcome these difficulties, and preliminary results are coming to hand. One of the objectives of this experiment is to obtain accurate measurements for comparison with the simulations.

There are three requirements in the relationship between the experiment and the simulation. Firstly, the Reynolds number must be matched precisely. Secondly, the experiment and simulation must have closely matched initial conditions. Following a suggestion by Inman and Bradshaw (1981), a mildly favorable pressure gradient is used to very closely approximate a self-preserving layer, i.e. by careful experimental design the boundary layer is maintained at almost constant thickness over some streamwise distance before being subjected to the APG. The FPG region allows the simulated layer and the experimental layer to approach each other without incurring a large increase in Re_θ which would reduce the streamwise extent of the simulations in the APG. In the experiment the additional development length has the added advantage of allowing upstream trip effects to decay before the region of interest. Finally, accurate experimental pressure coefficient (C_p) measurements with high spatial resolution are required

as an input for the simulation. A suitable flow configuration for the computations would be one in which the boundary layer experienced a non-dimensional pressure gradient $\beta = \frac{\delta^*}{\tau_w}\frac{dP}{dx} \approx 2$ at a maximum $R_\theta \approx 1500$. This design goal has been achieved.

2. Apparatus and methods

2.1. Tunnel and traverse

The layer develops on a 1m wide aluminium plate forming the test-section floor of a small open-return wind tunnel. The plate is supported above an optics table which also serves as an extremely flat and rigid mounting platform for a high-speed computer controlled 3D probe traverse. A flexible ceiling is contoured to produce the pressure distribution and two plexiglass sidewalls complete the test-section.

Selection of a transition device was performed in the absence of the PG. The incoming layers are laminar and closely follow the Blasius profile over an entrance velocity range from 6 to 12m/s. Various transition devices were tried, including 3D roughness, but a d=2.4mm wire located at X=0.15m was best, producing a "normal" turbulent boundary by X=0.35m. The Reynolds number per unit length based on the entrance velocity to the test section is 4.28×10^5 1/m giving a nominal entrance velocity of around 6.5 m/s. The Reynolds number was maintained constant to within $\pm 1\%$ during all measurements. The free-stream turbulence intensity in the test-section near the exit of the contraction is 0.25%.

The Y-axis (normal to the wall) of the traverse is carried by the (spanwise) Z-axis which is supported within the test-section by a gantry constructed of carbon-fiber composite. The Y- and Z- axes use linear stepping motors for positioning. Rubber strips are used to seal the gaps between the edges of the plate and the sidewalls. These gaps provide access for mounting the gantry to carriages underneath the plate. A brushless linear d.c. motor is attached to one of these carriages for positioning of the (streamwise) X-axis. The coordinate origin is on the wall at the centerline of the contraction exit. The size and repeatability of the measurement volume and the maximum traversing speeds are 2100 $\pm$ 0.1 mm at 2.0 m/s in the X-direction, 95 $\pm$ 0.05mm at 1m/s in the Y-direction and 500 $\pm$ 0.05mm at 1m/s in the Z-direction. These traversing speeds are sufficient for "flying hot-wire" measurements in regions of high turbulence intensity (see Watmuff, Perry and Chong 1983), but this capability has not been exploited yet.

2.2. Probes

Three round Pitot tubes with o.d. ranging from 1mm to 2mm are used to measure the mean velocity (U), and nine different Preston tubes with diameters ranging from 1.5mm to 7.9mm are used for skin friction coefficient (C_f) measurements.

Modified Dantec normal and cross-wire probes are used for the turbulence measurements. The distance between the prongs is reduced, and the prongs are stiffened with the addition of a small web. Platinum filaments 2.5 μm diameter and 0.5mm long are used. Perry, Lim, Henbest and Chong (1983) found substantial differences between profiles of $\overline{uv}$ measured in a rough-wall boundary layer where large turbulence intensities exist. The differences in $\overline{uv}$ were found to depend on the included angle between the cross-wire filaments and on whether the probe was stationary or "flying" upstream. The differences between the stationary and flying results were substantial only for conventional probes where the included angle is nominally 90°. Only small differences were observed when the included angle was increased to 120°. By tilting the probes in a uniform stream, Perry et al. found that a flow angle of 45° could be imposed on the probe with the 120° included angle without appreciable error, but that the probe with a 90° included angle started to show errors at flow angles as low as 20°.

Since relatively high turbulence intensities are also experienced in the APG region in this experiment, the included angle between the cross-wire filaments was increased to 110° which is about the maximum possible angle considering the probe geometry. Estimates of the Probability Density Function of the instantaneous flow angle (θ) relative to $\overline{V}$ have been measured at various positions in the layer and $\Pr[-20° < \theta < 20°] > 0.995$ in the most strongly turbulent regions. Thus, the errors described by Perry et al. should be small in this experiment.

Wall distances are set using the electrical contact of a needle with the test plate. This distance is calibrated by focussing a telescope on the filament and its image in the wall.

2.3. Methods

The small pressure differences in the test section (0.100 inches of water maximum) are measured using a high accuracy commercially available pressure transducer with an advertised accuracy of better than 0.001 inches of water and a range of 0.5 inches of water. The 44 static wall taps, pitot tube and reference total and static pressures are connected to the transducer *via* a 48 port Scanivalve under computer control. A pause of 5 seconds is used after the connection before reading the transducer, and all averages are obtained over at least 90 seconds.

The C_p variation is shown in figure 1, and it acts as a simple data base for inferring the local static wall pressure for all pressure probe measurements. The C_p data base was created by simply averaging the results of a number of runs performed several months apart. There is no discernible trend in the data taken at the different times. Averaging periods of up to 15 minutes were found to be necessary to achieve smooth data.

When the pressure probes are on the wall, the pressure difference between the probe and the local static pressure can be very small owing to the low velocities

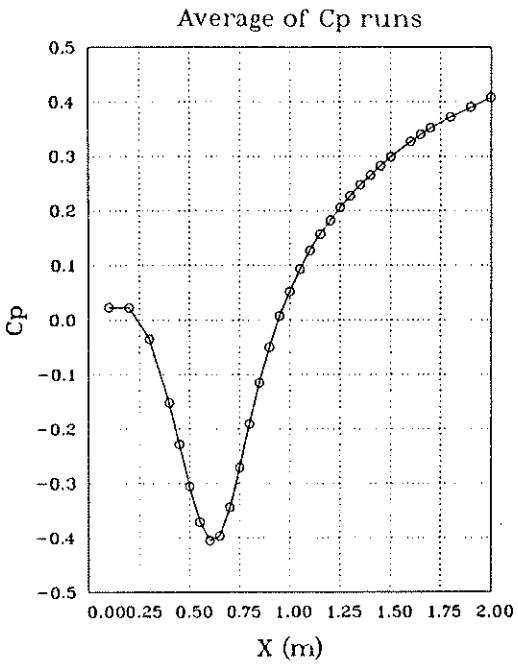

FIGURE 1. Variation of pressure coefficient C_p with X.

in the test-section. Further, the pressure difference is obtained by subtraction of two relatively large numbers. For the Preston tube C_f measurements, long time averaging periods were also necessary for smooth results.

Hot-wire probes must be calibrated frequently in a uniform stream. Using a conventional single-axis traversing system in this experiment would require the removal and reinstallation of fragile and expensive probes from the measurement region for the purpose of calibration. This would be time consuming and risk probe breakage. One advantage of the computer-controlled 3D traverse is that this operation occurs in a matter of seconds while minimizing the chances of probe damage. The system also acts as a shaker for imposing accurately known velocity perturbations on the cross-wire probes for calibration purposes.

A high-speed 15 bit Tustin A/D converter and a microVAX II computer are used for double-buffered data acquisition. A 32K hardware buffer is located between the Tustin and the computer and high speed DMA data transfers need only occur when the buffer is nearly full. While waiting for the new data the CPU is free to process data obtained during the previous data acquisition cycle using newly developed high-speed algorithms for reducing hot-wire data to Reynolds stresses, i.e. there is a high degree of parallelism between data acquisition and data processing. A system throughput of 25K/s for single wires and 10K/s for cross wires can be sustained indefinitely despite the fact that the calculations are performed in double-precision.

Total computer control of tunnel speed, probe traversal, and data acquisition allows all procedures to be automated. Sophisticated software enables long

duration experiments to be performed continuously over many days without manual intervention. This mode of operation required several significant new developments. For example, large and complex 3D measurement grids can be programmed and viewed ahead of time. Hot-wire calibration drift is monitored and new calibrations are performed (automatically) if the drift exceeds some tolerance. Other features that have proved vital for long duration unattended experimental runs include automatic error detection/recovery schemes and the provision of "emergency" asynchronous manually initiated software interrupts for hardware checkouts and to provide access to approximately 125 menu settable control variables.

Automation of the experiment allows massive quantities of data to be processed on-line over a relatively short period. Spatially dense mean-flow and Reynolds stress profiles are measured along the tunnel centerline at 50mm intervals from X=0.2m to X=2.0m, i.e. 37 profiles. The close spacing of the profiles is needed in the region of FPG to examine the recovery from upstream trip effects and the approach to self-similarity and in the region of APG where there is rapid growth with streamwise distance. The spacing of the profiles also provides a sensitive means for detecting anomalous data.

The greatest obstacle in obtaining high quality data has been hot-wire calibration drift caused by extremely large changes in ambient temperature. Variations of up to $40°F$ are typical over a 24 hour period while changes of up to $10°F$ have been observed over a period as short as 5 minutes. Automation of the experiment has provided a "brute force" solution to this frustrating problem, i.e. hot-wire profiles are repeated until the drift check obtained after measuring a profile is within a certain tolerance of a drift reference taken immediately after the wires have been calibrated. Setting the drift tolerance at 0.5% (larger tolerances introduce too much scatter in the data) has meant that on average a profile must be measured 5 times before it is acceptable. At the time of writing over 600 normal- and cross-wire profiles have been measured.

3. Results

3.1. Skin friction

The streamwise distribution of C_f at 37 streamwise locations along the tunnel centerline has been measured with 9 different diameter Preston tubes ranging in diameter from 1.5mm to 7.9mm In the FPG the larger diameter tubes protrude into the region where the mean flow deviates from the law of the wall. Downstream towards the end of the APG region the pressure difference ΔP between the smallest diameter probes and the local static pressure inferred from the C_p data base can be as small as 0.006 inches of water. Therefore, errors of 1% in the reference total head ($\approx$ 0.1 inches of water) or in the C_p data base lead to errors of $\approx$ 15% in ΔP. Consequently, the estimates from the 9 tubes have been averaged using the criteria that the nondimensional diameter $d^+ < 100$ and that

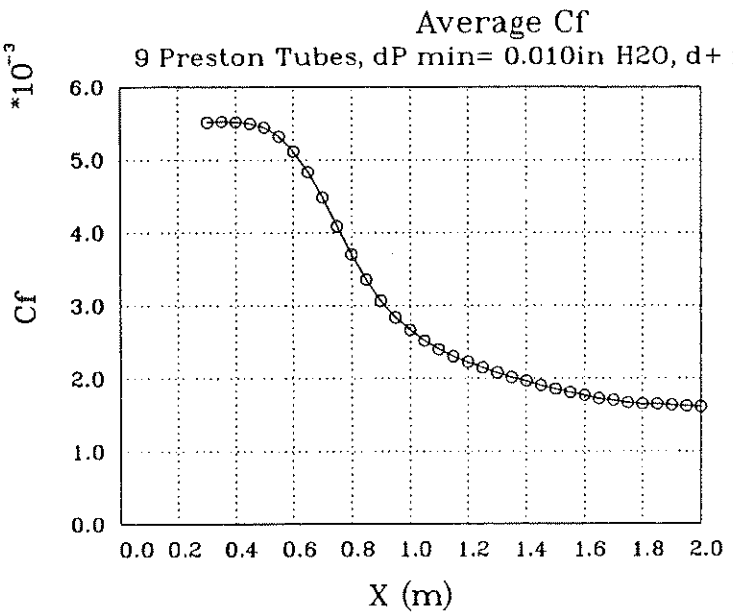

FIGURE 2. Skin friction coefficient C_f with X. Average of 9 different Preston tubes.

$\Delta P > 0.01$ inches of water. The averaged data are shown in figure 2. High values of $C_f (> 5.5 \times 10^{-3})$ are maintained in the FPG region. With application of the APG the C_f falls rapidly at first but for X>1.5m C_f approaches a constant value.

The accuracy of the C_f measurements needs to be considered since the pressure gradients in both the FPG and APG regions exceed the limits suggested by Patel (1965). Hirt and Thomann (1986) compared the wall shear stress τ_w measured directly with a floating element to values inferred from Preston tubes in axisymmetric boundary layers subject to sudden application and removal of adverse pressure gradients, i.e. the layers were far from equilibrium. Preston tube errors of up to 10% were observed. They found that the Preston tube readings indicated velocities below the law of the wall in decreasingly adverse pressure gradients. However, no parameters could be found to correlate the errors, so it is difficult to apply their results to this flow.

McDonald (1968) used empirical information combined with similarity arguments based on mixing length concepts to examine the effect of pressure gradient on the law of the wall. Deviations from the law of the wall were expressed as a function of a stress gradient $\alpha_0 = (\nu/\rho U_\tau^3) dP/dX$. In this experiment $-0.009 < \alpha_0 < 0.02$ and his results indicate that the deviations from the law of the wall may be as high as 8%. However, for a sink-flow the predictions indicate a negative deviation while the experiment of Jones and Launder (1972) and the numerical study by Spalart (1986) both indicate positive deviations from the law of the wall. Therefore, the accuracy of McDonald's predictions is questionable.

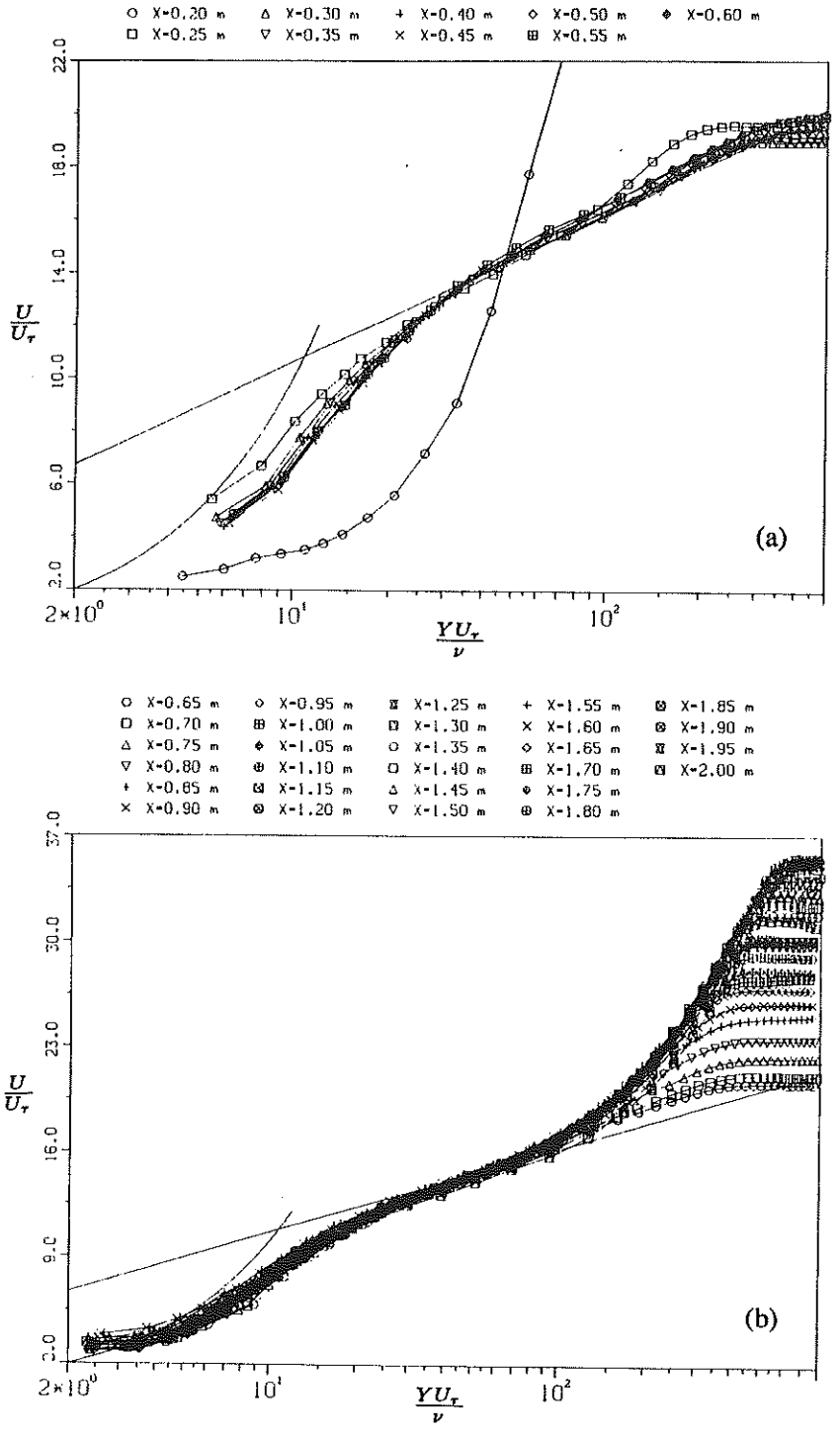

FIGURE 3. Mean velocity profiles with wall-scaling in (a) FPG region and (b) APG region. Hot-wire data.

In this experiment, the results from the 9 Preston tubes satisfying the averaging criteria described above cover the range $20 > d^+ > 100$ and the C_f estimates agree to within $\pm$ 3%. Moreover, the mean velocity profiles in the APG region shown in figure 3(b) (where $Y^+_{min} \approx 3$) fairly closely follow both the sublayer profile and the logarithmic law. The most significant anomalies appear in the FPG region, figure 3(a), where there are deviations from both the sublayer profile and the logarithmic law.

3.2. Mean velocity

It is well known that Pitot tubes suffer from wall proximity effects and a variety of correction schemes exist. However, it is uncertain which is the most appropriate for boundary layer data. Local static pressures have not been measured, and the Pitot tube data is reduced using the static pressure at the wall. The local static pressure throughout the layer could differ substantially from the wall static pressure owing to mean streamline curvature. Also, the Pitot tube mean flow data shows some scatter, especially in the near wall region, owing to the small pressure differences. For these reasons the normal hot-wire mean flow data are presented here.

The mean-velocity profiles in the FPG region are shown in figure 3(a). The first profile at X=0.2m (50mm downstream of the trip wire) is strongly contaminated by the trip. At X=0.25m the pressure gradient is small and the profile here has the appearance of a typical low Re_θ zero pressure gradient layer. Note the wake component. Also, this profile follows both the sublayer profile and the logarithmic law more closely than the other profiles. From X=0.3m onwards the profiles are essentially identical for about 20δ in the streamwise direction. The layer thicknesses $\delta \approx$ 12.0mm, $\delta^* \approx$ 1.75mm and $\theta \approx$ 1.2mm remain very nearly constant. At the end of the FPG the C_f is uniform to within $\pm 1\frac{1}{4}\%$ over a span of 40δ. These results provide strong evidence that the design goal of producing a highly 2D self-similar sink-like flow condition for compatibility with the initial conditions of Spalart's CFD simulations has been closely achieved. The small value of $Re_{\theta_{max}} = 650$ at the end of the FPG increases the size of the APG region which can be treated by the simulations.

Application of the APG increases the growth rate and the profiles become less full, resulting in large values of the strength of the wake component as shown in figure 3(b). The profiles appear to follow the law of the wall, but the region of logarithmic velocity variation remains small ($Y^+ < 100$). The layer thicknesses δ, δ^* and θ (not shown) increase almost linearly with streamwise distance and the profile shape factor H (not shown) is a weak indicator of the change. At the end of the region corresponding to Spalart's simulations (X=1m) $\delta \approx$ 28mm. The spanwise variation in C_f is within $\pm$3% over 12δ, and the momentum balance is within 5%. These results indicate that the layer is acceptably two-dimensional. The flow will provide an excellent test case for Spalart's new method since at X=1m, $Re_\theta \approx 1500$ and $\beta = \frac{\delta^*}{\tau_w}\frac{dP}{dx} \approx 2$.

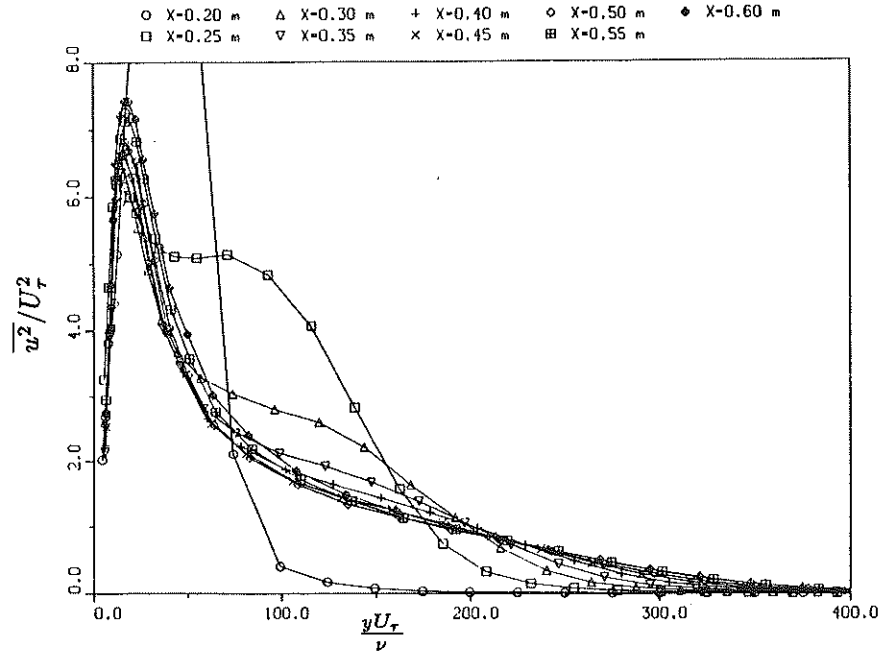

FIGURE 4. Streamwise development of $\overline{u^2}/U_\tau^2$ in the FPG region with wall scaling.

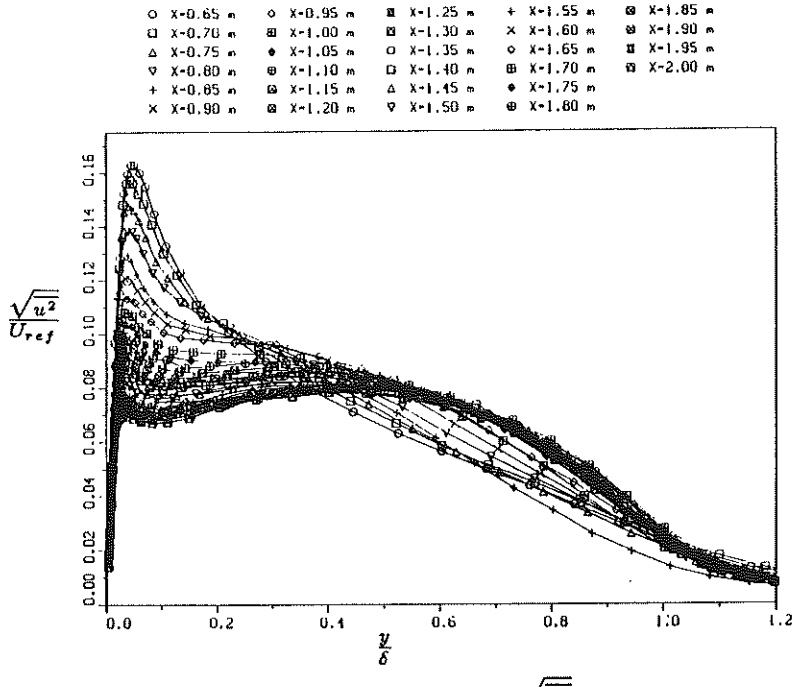

FIGURE 5. Streamwise development of $\frac{\sqrt{\overline{u^2}}}{U_{ref}}$ against $\frac{Y}{\delta}$.

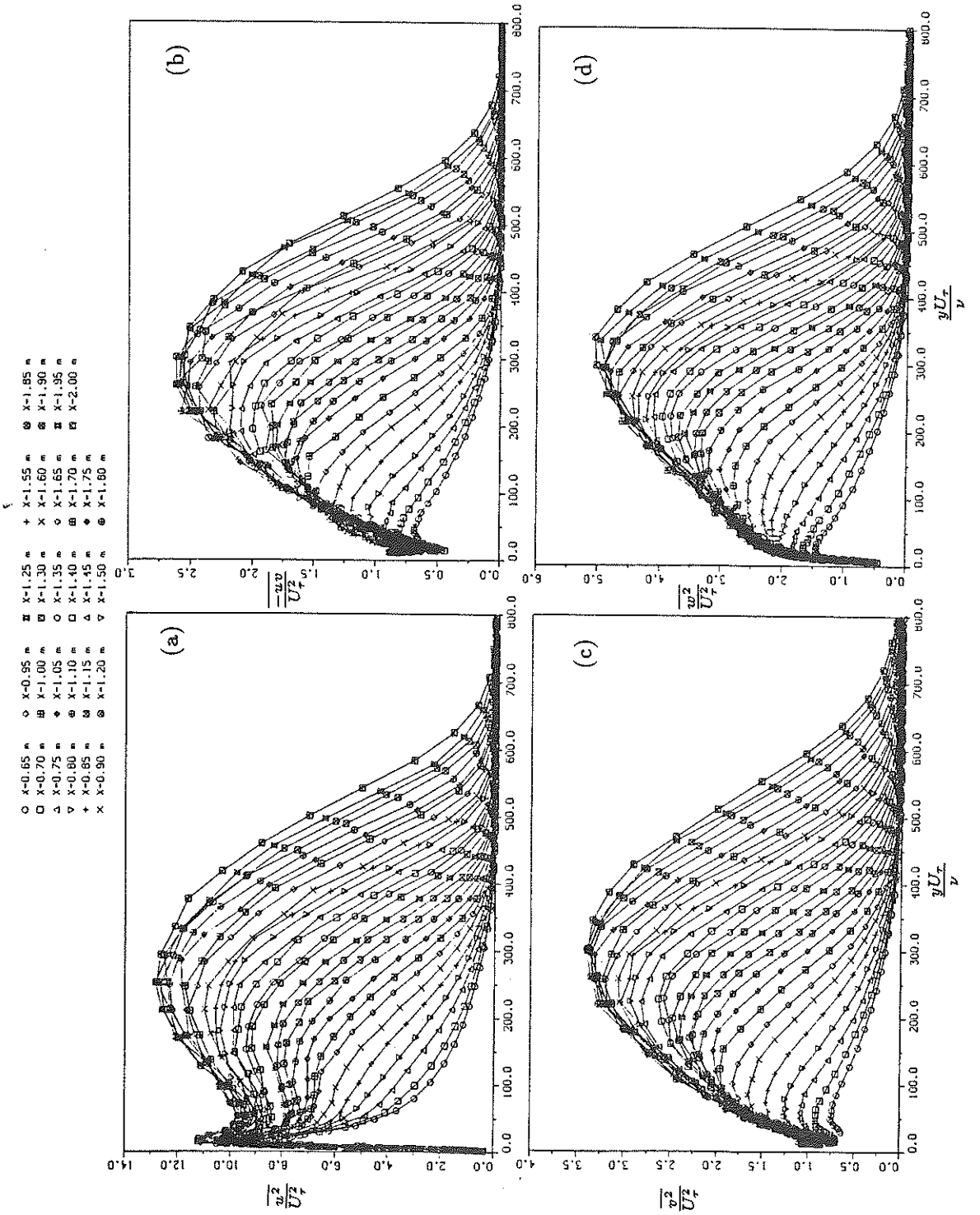

FIGURE 6. Streamwise development of Reynolds stresses in APG region in wall coordinates. (a) $\frac{\overline{u^2}}{U_\tau^2}$ (b) $\frac{\overline{-uv}}{U_\tau^2}$ (c) $\frac{\overline{v^2}}{U_\tau^2}$ (d) $\frac{\overline{w^2}}{U_\tau^2}$

Further downstream, in the region beyond the current capabilities of direct CFD simulations, there is evidence to suggest that the layer finally reaches a new self-preserving condition. Near the wall, the data follow the law of the wall, and in the outer region profiles of the velocity defect collapse. β approaches a constant value which is a necessary condition for self-preserving layers. Also, the strength of the wake component asymptotes to a constant value of around 14. Unfortunately, the two-dimensionality of the mean-flow is poorer in this region since the spanwise variation in C_f increases to $\pm 6\%$ and the momentum imbalance rises to about 9%.

3.3. Reynolds stress

The normal hot-wire measurements in the FPG region shown in figure 4 indicate that the trip effects decay rapidly in the near wall and outer regions but that a longer development length is required for recovery in the central region of the layer. However, the profiles have a marked similarity over the last 20δ of the FPG region. The same behaviour is observed for the cross-wire data $\frac{\overline{-uv}}{U_\tau^2}$, $\frac{\overline{v^2}}{U_\tau^2}$ and $\frac{\overline{w^2}}{U_\tau^2}$ but these results are not shown here. The observations provide further evidence that the layer is in a state of equilibrium before application of the APG.

Profiles of turbulence quantities in the APG region are shown with wall scaling in figures 6(a) to (d). The close spacing of the profiles provides a sensitive means of detecting inconsistencies in the data (assuming that the profiles should develop smoothly and monotonically with X). Large values of all the fluctuating quantities emerge in the central region of the layer with increasing streamwise distance. Note that $\frac{\overline{u^2}}{U_\tau^2}$ in the central region of the layer is larger than the peak value near the wall for $x > 1.5$m, in sharp contrast with channel flow and zero PG boundary layers.

Profiles of $\frac{\sqrt{\overline{u^2}}}{U_{ref}}$ are plotted against Y/δ in figure 5. Note that in the outer half of the layer the profiles are essentially identical for X > 1.1m. Similar observations apply for cross-wire data but these are not shown. It appears that the turbulent fluid in the outer region of the layer is convecting downstream almost without change. The peak values of the Reynolds stresses possess a locus which is linear with X, being inclined to the wall. The locus of maximum $\frac{\sqrt{\overline{u^2}}}{U_{ref}}$ can be clearly seen in the contour plot shown in figure 7(a). Contours of $\frac{\overline{u^2}}{U_\tau^2}$ are shown in figure 7(b). The disparity between the two sets of contours illustrates that the relationship between the turbulence structure at the wall and the outer flow varies widely in response to the pressure gradient. This is one of the most interesting aspects of this boundary layer.

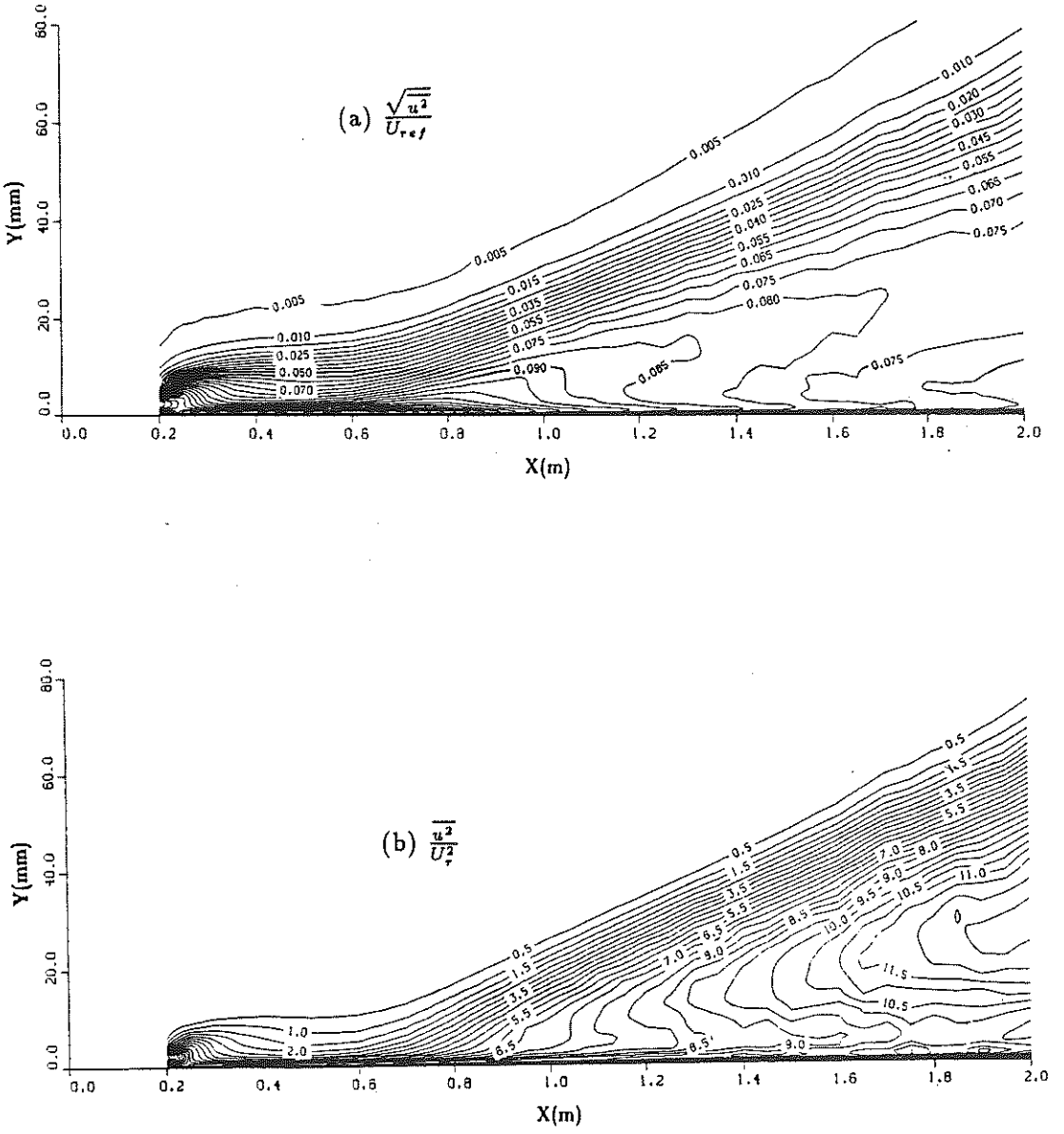

FIGURE 7. Contours of (a) $\frac{\sqrt{\overline{u^2}}}{U_{ref}}$, and (b) $\frac{\overline{u^2}}{U_\tau^2}$, throughout entire layer.

REFERENCES

HIRT, F. & THOMANN, H. 1986 Measurement of wall shear stress in turbulent boundary layers subject to strong pressure gradients. *J. Fluid Mech.* **171**, 547- 562.

INMAN, P. N. & BRADSHAW, P. 1965 Mixing length in low Reynolds number turbulent boundary layers. *AIAA J. Vol. 19, No. 5.* 653-655.

JONES, W. P. & LAUNDER B. E. 1972 Some properties of sink-flow turbulent boundary layers. *J. Fluid Mech.* **56**, 337-351.

MCDONALD, H. 1968 The effect of pressure gradient on the law of the wall in turbulent flow. *J. Fluid Mech.* **35**, 311-336.

PATEL, V. C. 1965 Calibration of Preston tube and limitations of its use in pressure gradients. *J. Fluid Mech.* **23**, 185-208.

PERRY A. E., LIM K. L., HENBEST S. M. & CHONG M. S. 1983 Rough- and smooth-walled shear flows. Fourth Symposium on Turbulent Shear Flows, Karlsruhe, F. R. G.

SPALART, P. R 1986 Numerical study of sink-flow boundary layers. *J. Fluid Mech.* **172**, 307-328.

SPALART, P. R. 1988 Direct simulation of a turbulent boundary layer up to Re_θ=1410. *J. Fluid Mech.* **187**, 61-98.

WATMUFF, J. H., PERRY, A. E. & CHONG, M. S. 1983 A Flying Hot-Wire System. *Experiments in Fluids.* Vol. 1. 1983.